JOURNAL OF GEOPHYSICAL RESEARCH, VOL. 105, NO. C10, PAGES 24,141–24,156, OCTOBER 15, 2000

Particle transport through a narrow tidal inlet due to tidal forcing and implications for larval transport

Cheryl A. Brown, George A. Jackson, and David A. Brooks

Department of Oceanography, Texas A&M University, College Station

Abstract. For estuarine-dependent species, especially those that spawn offshore and whose larvae must reach estuarine nursery areas, advective transport through tidal inlets may be a major factor influencing recruitment variability. We examined the role of tidal forcing on particle transport through a narrow, microtidal inlet along the Texas coast by using a three-dimensional hydrodynamic and particle transport model. Although tidal forcing is relatively small in the study area, tidal currents through the inlet effectively transport passive particles a distance of about 15 km landward of the inlet. The majority of the particles that enter the inlet are transported to regions that are not suitable for larval settlement. There is limited tidal dispersion of the particles into the bays due to shoreline geometry and bathymetry. Most of the particles that enter the inlet are expelled offshore in the ebb tidal jet resulting in estuarine-shelf exchange of particles. When acting alone, tidal forcing is not effective at retaining particles in a suitable estuarine habitat, suggesting that other physical or biological mechanisms are required to maintain larvae in an estuarine habitat or that there is substantial along-shelf transport of larvae.

1. Introduction

Estuarine environments compose only a small fraction of the Earth's surface. Despite their areal insignificance, estuaries form a crucial ecological habitat and serve as a nursery area for numerous animals, including commercially important fish species [*Hoss and Thayer*, 1993]. Estuaries are particularly important along the Atlantic and Gulf of Mexico coasts of the United States, where they extend along the majority of the coastline and where commercial fisheries rely heavily on estuarine-dependent species. Approximately 98% of the commercial fisheries catch in the Gulf of Mexico consists of estuarine-dependent species [*McHugh*, 1976], many of which must travel from spawning grounds located on the shelf to estuarine nursery areas. Fisheries recruitment to these nursery areas is highly variable because of a combination of biotic and physical factors resulting in major ecological and economic consequences. Variations in larval supply associated with advective transport can be a critical factor influencing recruitment for animals in general [e.g., *Norcross and Shaw*, 1984; *Cowen*, 1985; *Roughgarden et al.*, 1988; *Hamer and Jenkins*, 1997; *Jenkins et al.*, 1997]. For species that spawn offshore and have estuarine nursery areas, currents carrying them through inlets and retention in estuarine nursery areas may control larval supply and recruitment variability [*Jenkins and Black*, 1994; *Jenkins et al.*, 1997]. Water movement also determines the fate of other material in estuaries, such as nutrients, contaminants, and suspended sediment.

Movement through inlets results from the interaction of astronomical tides, freshwater discharge, meteorological forcing, and nontidal sea level changes. The dominant physical processes vary spatially. The inner shelf (inside the 20-m isobath) is influenced by strong tidal currents and tidal mixing, wind-driven circulation, and buoyant discharges with associated features, such as plumes and fronts. Near tidal inlets, the circulation patterns are complex owing to strong tidal currents, tidal residuals, and bathymetric features, such as dredged channels, sills, shoals, and deltas [*Werner et al.*, 1997]. Small-scale features, such as eddies and fronts, often dominate the flow field near the inlet.

Because of the temporal and spatial variability in physical processes and larval abundance, sampling limitations make it difficult to interpret larval abundance data, to discern the dominant processes influencing recruitment, and to infer large-scale recruitment patterns. Numerical models of larval transport provide a means of examining the role of various physical and biological processes influencing recruitment and may aid in the sampling design for larval studies [*Colby*, 1988; *Werner et al.*, 1997].

Numerical models have provided insight into the mechanisms influencing the transport of fish larvae in shelf and coastal regions [e.g., *Werner et al.*, 1996, 1999]. There have been relatively few models developed for transport of fish larvae from shelf regions through inlets to estuarine nursery areas [*Jenkins and Black*, 1994; *Jenkins et al.*, 1997; *Luettich et al.*, 1999; *Xie and Eggleston*, 1999]. Most such models treat larvae as passive particles that emphasize the importance of currents. Utilizing a hydrodynamic and Lagrangian particle transport model, *Jenkins and Black* [1994] found that the temporal variability in settlement of the fish *Sillaginodes punctata* within Port Phillip Bay, Australia, is determined by low-frequency hydrodynamic events. Based on particle transport and wave generation models, *Jenkins et al.* [1997] suggested that the majority of the variation in recruitment within Port Phillip Bay could be explained by the supply of larvae associated with advective transport and disturbance of settlement sites by wave action. Simulations of fish larval transport for Beaufort Inlet, North Carolina,

Paper number 2000JC000211.
0148-0227/00/2000JC000211$09.00

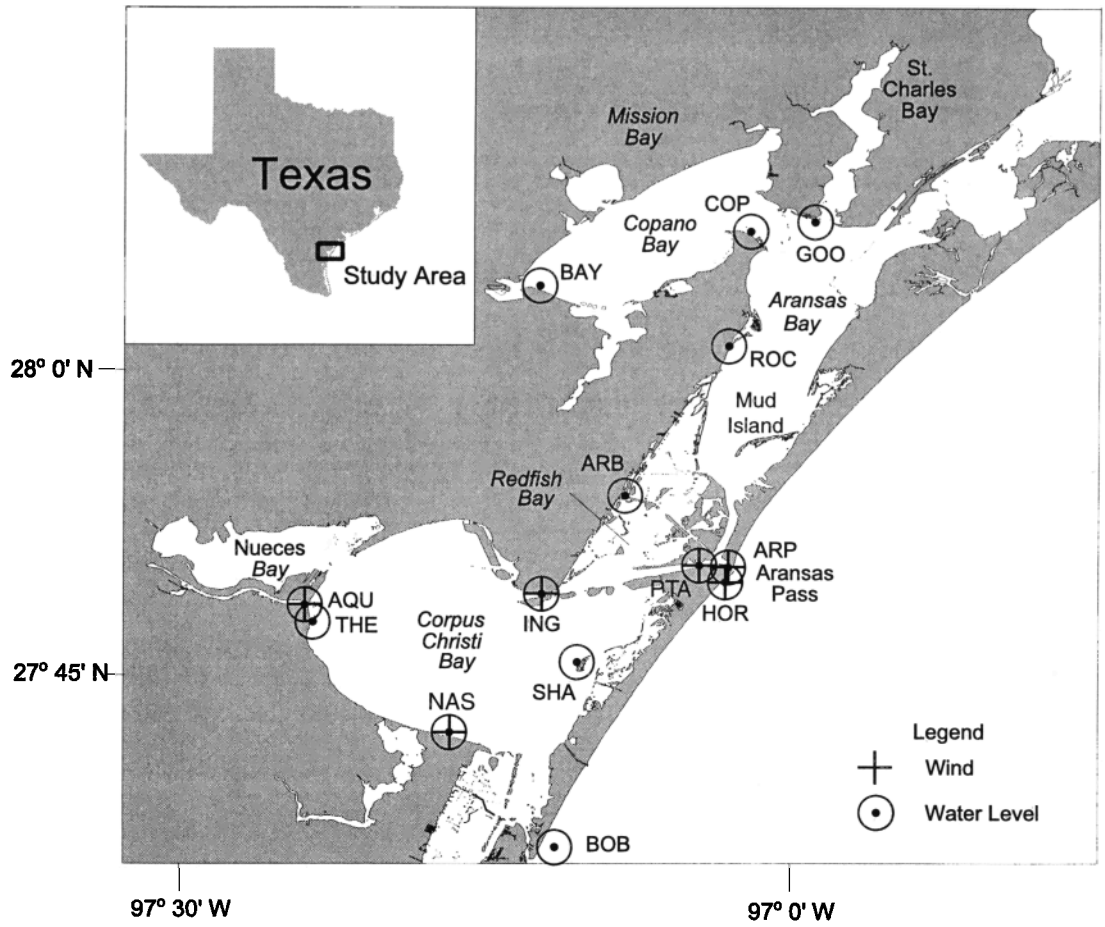

Figure 1. Location map of study area with symbols indicating locations of stations.

indicated that particle transport pathways depend on particle release locations [*Luettich et al.*, 1998, 1999]. Tidal currents are effective at transporting larvae into this inlet; however, only a limited number of wind directions enhance larval ingress through the inlet. Model simulations suggest that a fraction of the larvae may be retained in a residual eddy over the ebb tidal delta outside Beaufort Inlet. *Smith and Stoner* [1993] modeled the transport of larvae through Aransas Pass on the basis of predicted inlet current velocities and vertical larval concentration (including vertical migration and turbulent mixing). Simulations indicated that diel vertical migration resulted in an annual cycle in larval ingress, but nontidal transport dominated the transport.

Inlet geometry, bathymetry, and details of particle release (time and place) cause substantial variation in particle transport [*Kapolnai et al.*, 1996; *Wheless and Valle-Levinson*, 1996; *Luettich et al.*, 1998]. Because of the importance of inlet geometry and variability, models need to be developed that include realistic bathymetry and shoreline configuration in order to obtain accurate representations of particle transport and dispersion at small scales for a given inlet system [*Geyer and Signell*, 1992; *Kapolnai et al.*, 1996].

We are applying a numerical model to investigate the transport of larvae through Aransas Pass to estuarine nursery areas. Aransas Pass (Figure 1) is an important inlet along the Texas coast because it serves as the primary Gulf of Mexico connection for numerous Texas bays and provides access to these bays for many commercial and recreational fisheries. This is the first part of a study investigating the dominant physical and biological processes that influence the recruitment of red drum (*Sciaenops ocellatas*) to estuarine nursery areas in the region. Red drum spawn in the evenings from late August to early October in the vicinity of tidal inlets [*Holt et al.*, 1985]. When the larvae are 2-3 weeks old, they can settle in estuarine nursery grounds, primarily sea grass habitats [*Holt et al.*, 1983; *Rooker and Holt*, 1997; *Rooker et al.*, 1999]. The larvae depend upon currents to transport them through Aransas Pass and to a suitable estuarine habitat. Although this study focuses on the transport of red drum larvae, the results may be applied to other species with similar life histories.

The objectives of this paper are to characterize the tides within the study area, assess the performance of the model at simulating the tides in a microtidal region, and investigate the role of tidal forcing on larval transport through the Aransas Pass inlet. We examine the transport of larvae over short timescales (<6 tidal cycles), including examination of the source region for particles that enter the bays, maximum tidal excursions, tidal dispersion of particles, and particle retention within the bays.

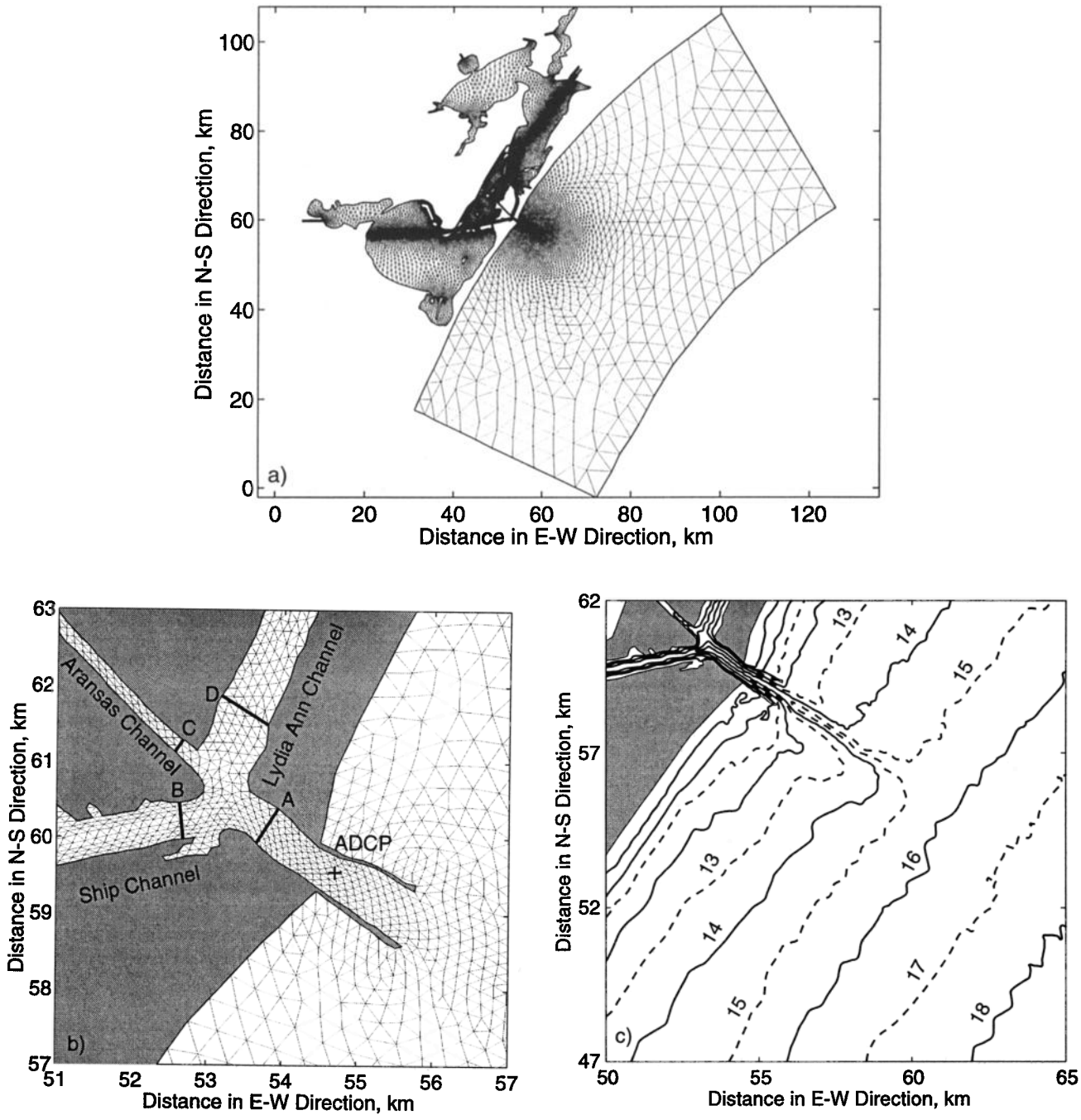

Figure 2. Mesh of (a) study area showing (b) details of the inlet and location of transects for acoustic Doppler current profiler (ADCP) comparisons, and (c) bathymetry outside the inlet indicating the presence of a shoal south of the inlet.

2. Description of Study Area

Aransas Pass is a narrow inlet (400-500 m wide) located along the central Texas coast in the northwestern Gulf of Mexico. The nearest adjacent inlets are Pass Cavallo to the north and Mansfield Pass to the south, both of which are approximately 100-150 km from Aransas Pass. The original bathymetry and shoreline configuration of the study area have been modified by the dredging of channels, emplacement of jetties, and creation of islands, all of which influence the circulation in the inlet and bays [*Powell et al.*, 1997]. Aransas Pass has jetties that extend about 1 km from the shore to the 10-m depth contour. After passing through the inlet from the Gulf of Mexico, water is directed into one of three channels: the Corpus Christi (CC) Ship Channel (14 m deep and 120 to 180 m wide), the Aransas Channel (4 m deep and 40 m wide), and Lydia Ann Channel (5 to 7 m deep and 200 to 300 m wide near the entrance decreasing to a depth of 4 m and a width of 40 m in Aransas Bay); (Figure 2). Aransas Pass serves as the Gulf of Mexico connection for six shallow bays, including Corpus Christi, Nueces, Aransas, Redfish, Copano, and St. Charles Bays, which have a

combined surface area of 1100 km^2 and mean depths of 3.6, 0.7, 2.4, 1.2, 2.2, and 1.0 m, respectively [*Ward*, 1997].

Tides provide an important driving force for exchange through the inlet. In the Gulf of Mexico, the tides are primarily diurnal or mixed diurnal-semidiurnal [*Zetler and Hansen*, 1970; *Marmer*, 1954]. The dominant diurnal tides (K_1 and O_1) in the Gulf of Mexico co-oscillate with those in the Atlantic and are driven by the in-phase flow through the Straits of Florida and Yucatan Channel [*Reid and Whitaker*, 1981]. The dominant semidiurnal constituent, M_2, is primarily generated within the Gulf of Mexico by astronomical forcing and propagates cyclonically around the gulf as a Kelvin wave [*Reid and Whitaker*, 1981; *Reid*, 1990]. The amplitudes of the dominant diurnal constituents, K_1 and O_1, are approximately 15 cm in the Gulf of Mexico adjacent to Aransas Pass; the amplitudes of the dominant semidiurnal constituents, M_2 and S_2, are 8 and 2 cm, respectively [*Zetler and Hansen*, 1970; *Marmer*, 1954; *DiMarco and Reid*, 1998].

The channels that connect the bays to the coastal ocean filter the tidal motions, preferentially attenuating the semidiurnal constituents [*Smith*, 1974]. Although the tides in the study area are relatively small, they regularly produce peak current velocities at Aransas Pass of about 1.5 m s^{-1} [*Williams et al.*, 1991]. There is minimal vertical salinity stratification (<0.5 ppt m^{-1}) in the bays due to limited freshwater inflows, shallow depths, and strong local wind forcing. However, a north-south salinity gradient exists, with lowest salinities in the Aransas-Copano Bay region [*Ward*, 1997].

3. Methodology

The present study has three components: (1) analysis of tidal data to determine the amplitude and phase of tidal constituents in the surrounding bays, (2) application of a coastal circulation model to describe regional flow and testing the model results against observations, and (3) simulation of particle transport between the coastal ocean and the bays.

3.1. Data Analysis

Principal tidal constituents were computed by analyzing water level data for 14 stations within the study area (Table 1, Figure 1). Water level data have been collected with the Texas Coastal Ocean Observation Network (TCOON) operated by the Conrad Blucher Institute for Surveying and Science, Texas A&M University–Corpus Christi [*Michaud et al.*, 1994]. Water level data were recorded at 6-min intervals (except for ARB and ARP which were at 60-min intervals) to National Ocean Service (NOS) standards by using the Next Generation Water Level Measurement Systems. We computed amplitudes and phase lags of the sea surface elevation tidal constituents by using a tidal analysis code [*Foreman*, 1977]. The data were 3- and 40-hour band-pass filtered and resampled hourly. Data gaps in the record of less than 6 hours were filled by linear interpolation; gaps longer than 6 hours were not filled. For years between 1993 and 1998 that contained less than 5% missing data, the tidal analysis was performed on 1-year-long time series (except ARP and ARB, which only had 6-month time series available). Mean and standard deviation of the amplitude and phase lag of the dominant tidal constituents were computed for each station.

Table 1. Station Names and Positions

Station Name (Abbreviation)	Latitude/ Longitude	Source of Data
Aquarium (AQU)	27.82°N / 97.40°W	TCOON
Aransas Bay (ARB)	27.90°N / 97.14°W	NOS
Aransas Pass (ARP)	27.84°N / 97.05°W	NOS
Bayside (BAY)	28.07°N / 97.20°W	TCOON
Bob Hall Pier (BOB)	27.58°N / 97.22°W	NOS
Copano Bay (COP)	28.12°N / 97.03°W	TCOON
Goose Island (GOO)	28.13°N / 96.98°W	TCOON
Ingleside (ING)	27.82°N / 97.20°W	TCOON
Naval Air Station (NAS)	27.71°N / 97.28°W	TCOON
Offshore (OFF)	27.93°N / 96.17°W	TCOON
Port Aransas (PTA)	27.84°N / 97.07°W	TCOON
Rockport (ROC)	28.02°N / 97.05°W	TCOON
Shamrock (SHA)	27.77°N / 97.15°W	TCOON
T-head (THE)	27.80°N / 97.39°W	TCOON

TCOON, Texas Coastal Observation Network; NOS, National Ocean Service.

3.2. Circulation Model

Tidal circulation patterns were computed by using a three-dimensional, free surface, nonlinear finite-element model described by *Lynch and Werner* [1991] and *Lynch et al.* [1996]. Spatially and temporally variable horizontal eddy diffusion coefficients were parameterized by following *Smagorinsky* [1963]. Vertical mixing was parameterized by using the level-2.5 turbulence closure model [*Mellor and Yamada*, 1982; *Galperin et al.*, 1988]. Since the water column in the study area is typically well mixed, baroclinic forcing was neglected. Bottom friction was represented by using a quadratic slip condition with a uniform drag coefficient of 0.005. No attempt was made to vary the drag coefficient in space to account for variations in bottom types.

3.2.1. Model domain. The model domain encompassed Corpus Christi, Nueces, Redfish, Copano, Mission, and St. Charles Bays and extended 50 km offshore to the 50-m depth contour (Figures 1 and 2). The shoreline configuration of the study area is complex, including numerous islands and intersecting channels. The study area was represented with a variable resolution linear triangle, finite-element mesh, which included 14,300 nodes and 26,291 elements. Nodal spacing varied from about 7 km in the shelf region to about 50 m within the inlet (Figure 2). Bathymetry used to generate the mesh was obtained from National Ocean Survey and the U.S. Army Corps of Engineers, Galveston District. The jetties extending from the pass into the Gulf of Mexico were included in the mesh. A model time step of 10 s kept the Courant number ($C_n \equiv u\,\Delta t / \Delta x$, where u is the fluid velocity, Δt is the model time step, and Δx is the spatial grid scale) less than approximately 0.1. The vertical mesh consisted of 11 uniformly spaced nodes under each horizontal grid point.

3.2.2. Boundary and initial conditions. Results of previous studies [*Zetler and Hansen*, 1970; *DiMarco and Reid*, 1998] and our analysis of water level data from stations in the shelf region indicate that the phase lags of the tides in the northwestern Gulf of Mexico are essentially uniform. Between Port Isabel and Freeport, Texas (along-shelf distance of approximately 400 km), the phase lag of the dominant diurnal constituents (K_1 and O_1) differ by less than 1° while

Table 2. Comparison of Amplitude (Amp.) and Phase Lag of Sea Surface Height Tidal Constituents for Stations in the Northwestern Gulf of Mexico

Station	K_1		O_1		M_2		Study
	Amp., cm	Lag, deg	Amp., cm	Lag, deg	Amp., cm	Lag, deg	(Latitude/Longitude)
BOB	15	25	15	17	8	260	this study
OFF	15	24	15	17	7	258	this study
Port Aransas	15	26	15	20	8	262	*Zetler and Hansen* [1970] (27.83°N / 97.06°W)
Port Isabel	14	25	15	20	7	256	*Zetler and Hansen* [1970] (26.06°N / 97.15°W)
01	16	25	15	16	8	260	*DiMarco and Reid* [1998] (27.26°N / 97.25°W)
23	15	25	15	16	9	268	*DiMarco and Reid* [1998] (28.71°N / 95.54°W)

the phase lag of the M_2 constituent varies by 12° (Table 2). In addition, simulations of the tides in the Gulf of Mexico indicate that the phase lag of the K_1 and O_1 constituents differ by less than 1° and the phase lag of the M_2 constituent differs by 2° over the shelf portion of the study area [*Westerink et al.*, 1993]. Because of the uniform tidal movement over the region, the amplitude and phase of the surface elevation along the offshore boundaries (including cross-shore boundaries) were imposed as spatially constant. A "no normal flow" boundary condition was applied at all the coastline boundaries. Model simulations began with the model domain at rest; tidal forcing was increased linearly over three tidal cycles. To characterize the tides in the study area, simulations were performed for the dominant tidal constituents (K_1, O_1, P_1, and M_2), both independently and combined.

3.2.3. Comparison with data. To assess the performance of the model, tidal amplitude and phase lag, depth-integrated discharge, and current velocities were compared with observations. We compared simulated discharges through the inlet and three channels (CC Ship, Lydia Ann, and Aransas) to observed discharges. The observational estimates were calculated from acoustic Doppler current profiler (ADCP) transects of the channels (locations presented in Figure 2b as lines A-D) performed once per hour during a 3-day period from June 21 to June 24, 1994 by the Texas Water Development Board (R. Solis, personal communication, 1998). We estimated the tidal forcing during June 11-25, 1994, by using the tidal constituents computed at BOB for 1994. Tidal forcing was applied at the offshore boundary as a water elevation. In addition, we compared simulated velocities in the ship channel inside the inlet with those obtained from a bottom-mounted ADCP (location shown in Figure 2b) deployed from April 9 to May 8, 1990 [*Williams et al.*, 1991]. We estimated the tidal forcing during this interval by using the mean amplitude and phase lag for the dominant tidal constituents computed for BOB from 1994 to 1998 (see Table 3). Tidal ellipses were computed by using the tidal analysis code of *Foreman* [1978].

3.3. Particle Transport

To examine the role of tidal forcing on larval transport, we introduced particles into the model and tracked them throughout the model domain by using a fourth-order Runge-Kutta scheme [*Blanton*, 1995]. Passive particles were

Table 3. Mean amplitude (Amp.) and Greenwich Phase Lag of Water Elevation for Dominant Diurnal and Semidiurnal Tidal Constituents (Standard Deviation in Parentheses) and Number of Years (*n*) of Data Included in the Analysis

	K_1		O_1		P_1		M_2		
Station	Amp., cm	Lag, deg	Amp., cm	Lag, deg	Amp., cm	Lag, deg	Amp., cm	Lag, deg	*n*
BOB	15.0 (03)	24.5 (0.4)	15.1 (0.2)	17.0 (0.7)	4.6 (0.2)	27.8 (2.0)	7.8 (0.1)	260.2 (0.9)	6
OFF	15.4	24.4	15.1	17.1	5.0	23.6	7.2	258.1	1
ARP	11.0	32.7	11.0	26.2	--	--	6.6	250.8	0.5
PTA	9.4 (0.3)	38.4 (1.2)	9.5 (0.2)	31.9 (1.0)	2.8 (0.2)	36.0 (2.8)	5.0 (0.1)	257.3 (0.9)	5
ING	5.9 (0.1)	96.9 (1.7)	6.3 (0.2)	87.5 (1.3)	1.6 (0.1)	98.1 (2.5)	1.4 (<0.1)	354.7 (1.8)	6
NAS	6.2 (0.1)	106.4 (1.2)	6.5 (0.2)	95.7 (1.0)	1.8 (0.1)	109.8 (2.0)	1.6 (<0.1)	19.7 (1.6)	5
AQU	6.3 (0.1)	110.0 (1.0)	6.5 (0.2)	95.4 (0.6)	2.0 (0.1)	115.6 (1.0)	1.7 (<0.1)	17.4 (1.0)	4
THE	5.9	107.9	6.2	96.2	1.8	111.3	1.7	18.2	1
SHA	6.2	105.8	6.2	97.6	1.5	102.1	1.5	23.7	1
ARB	5.1	81.2	5.4	74.6	1.3	85	1.8	309.5	0.5
ROC	2.9 (0.1)	105.7 (1.8)	3.0 (0.1)	100.2 (2.1)	0.8 (<0.1)	99.8 (4.5)	0.7 (<0.1)	329.5 (2.1)	6
COP	3.0 (0.1)	116.1 (6.2)	3.3 (0.2)	110.3 (6.5)	0.7 (0.1)	114.4 (8.8)	0.8 (<0.1)	5.6 (17.5)	6
BAY	3.4 (0.3)	141.9 (0.8)	3.5 (0.2)	127.1 (2.8)	1.3 (0.1)	145.1 (12.5)	1.0 (0.1)	48.3 (4.7)	3
GOO	2.4	119.7	2.8	120.7	0.7	127.4	0.6	10.5	1

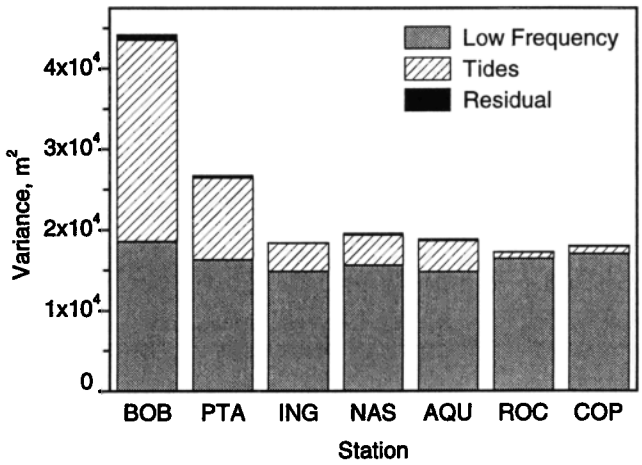

Figure 3. Variance of water level height associated with tidal and low-frequency motions. Offshore of the inlet, the water level variance is equally distributed between tidal and low-frequency processes. Low-frequency water level motions propagate into the bay with little attenuation, while tidal motions are rapidly attenuated. Station locations are shown in Figure 1.

released in the vicinity of the inlet during different stages of the tidal cycle under various tidal forcing conditions. Particles were released in the model domain in three different configurations. To determine the source region of particles that enter the inlet during one flood tide, 4772 passive particles were released in a rectangular region (4.5 km by 6 km) offshore of the inlet mouth. The source of particles that enter the inlet over multiple tidal cycles was examined by releasing additional particles (33,571 particles) over a larger offshore region (17.9 km by 10.4 km) at the same density as that for the previous case. To examine the effect of varying particle release location, 3360 particles were released inside the inlet at the beginning of flood tide. For all configurations, particles were released at the beginning of flood tide during tropic tides (period of maximum diurnal range) for $K_1 + O_1 + P_1$ forcing to obtain maximum particle excursions and particle retention within the bays. The particles were released 0.5 m below the surface with their depth held constant throughout the simulation (vertical velocity equal to zero) and particles were tracked for 6 tidal cycles. Additional simulations were performed by releasing neutrally buoyant particles 2 and 5 m below the surface. Results for all particle release depths were similar; therefore only results for particle release at 0.5 m are presented.

4. Results

4.1 Water Elevation and Currents

4.1.1. Analysis of tidal records. We computed the variances associated with tidal and low-frequency motions for seven stations (BOB, PTA, ING, NAS, AQU, ROC, and COP) by using time series of water level data from 1994 (Figure 3). We determined the contribution of tides by using the tidal amplitudes and phase lags of constituents to predict the tides and computed the variance of the predicted tides. The low-frequency component represents the variance of the record after a 40-hour low-pass filter. The residual represents the component of the 3- to 40-hour band not associated with tidal motions. At the nearshore location (BOB), the water level variance is approximately equally distributed between tidal and low-frequency (periods longer than 40 hours) processes. Except for locally generated setup and setdown, low-frequency water level variations within the bays occur primarily in response to estuarine-shelf exchange driven by changes in coastal sea levels [*Smith*, 1978]. These low-frequency water level motions propagate into the bays with little attenuation, in contrast with the tidal motions, which are rapidly attenuated. Tidal variance decreases by more than 50% inside the inlet (PTA) and is essentially absent at the Rockport and Copano stations.

Tidal motion accounts for the majority of the water level variance within the 3- and 40-hour band. In the nearshore region outside the inlet (e.g., BOB), tides account for 97% of the variance within the 3- and 40-hour band, and the dominant tidal constituents (K_1, O_1, P_1, M_2) account for 95% of the total tidal variance. In contrast, analysis of current records in the shelf region of the study area shows that only

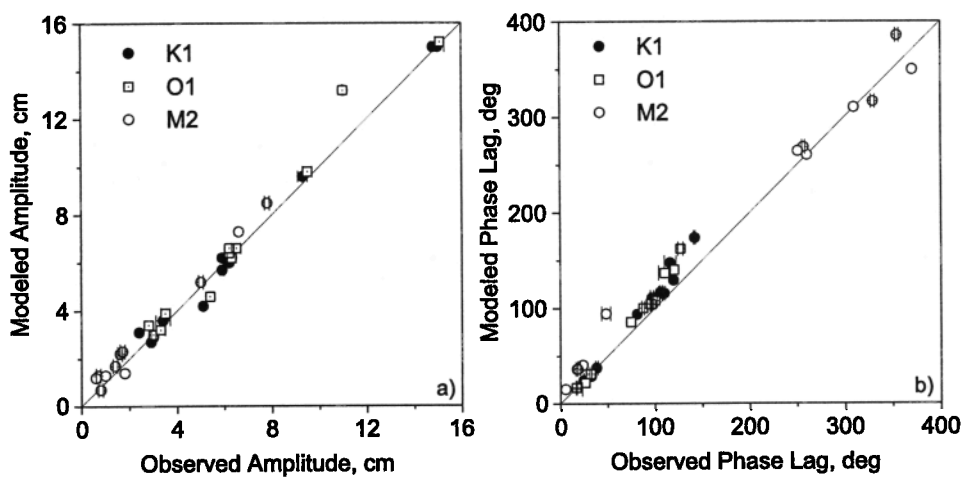

Figure 4. Comparison of modeled and observed (a) amplitude and (b) phase lag of the dominant tidal constituents (K_1, O_1, and M_2). Error bars represent standard deviation of amplitude and phase lag (see Table 3). The RMS differences of modeled and observed amplitude and phase lag are about 1 cm and 15°, respectively.

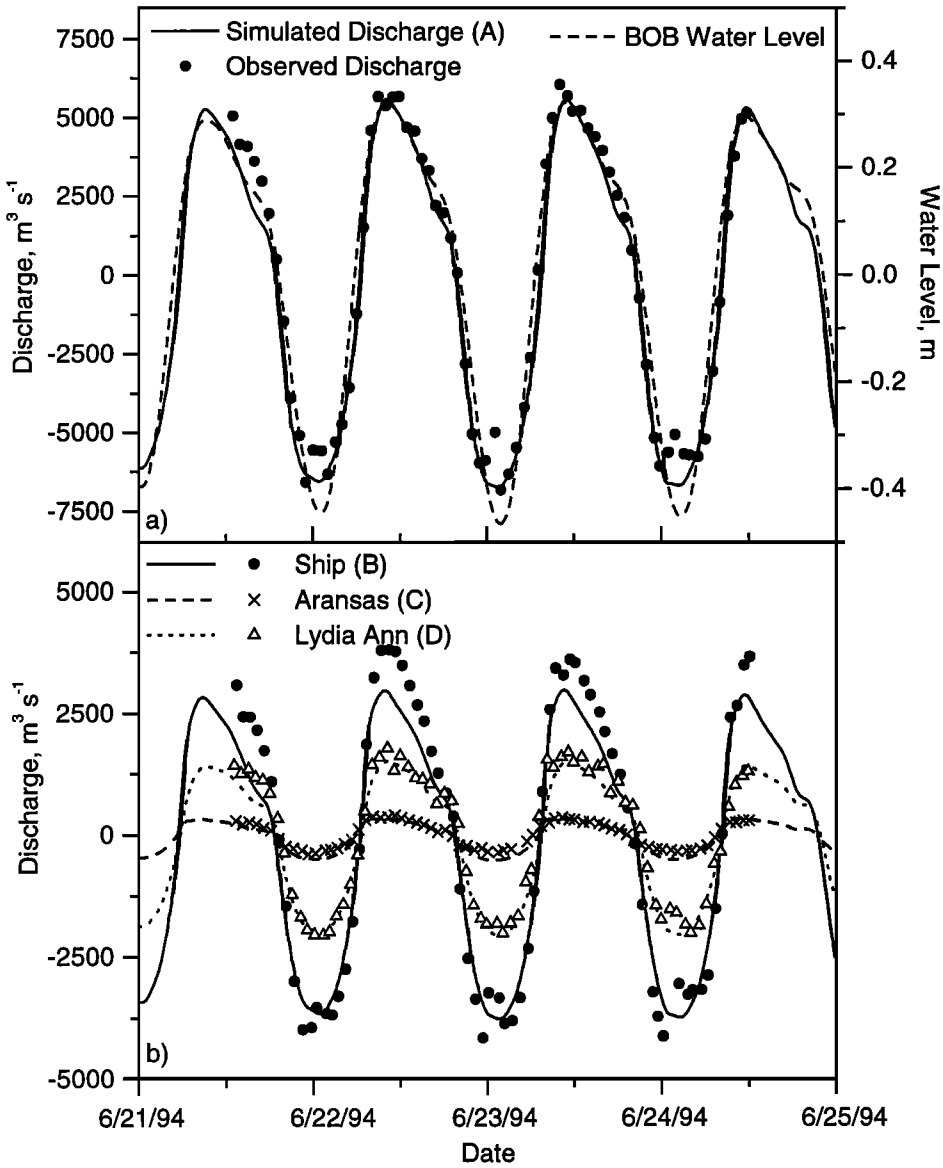

Figure 5. Comparison of simulated and observed discharge (a) through the inlet and (b) in three channels (location of the transects are shown in Figure 2) with positive values corresponding to flood tide.

approximately 10-20% of the energy in the 8- to 40-hour band is associated with tidal motions [*DiMarco and Reid*, 1998].

4.1.2. Comparison between modeled and observed water surface elevation. The root-mean-square (RMS) difference between the modeled and observed amplitudes of the water surface elevation for the dominant diurnal and semidiurnal constituents (K_1, O_1, M_2) is less than 1 cm, and the maximum difference is about 2 cm (Table 3, Figure 4a). The location with the largest discrepancy is the Aransas Pass (ARP) station, which has less than 1 year of data available for the tidal analysis. Furthermore, it is located in a region where the tidal amplitudes are rapidly attenuated and small changes in station position or local bathymetry can have large effects on measured or calculated amplitudes.

The RMS difference between the simulated and observed phase lags of water surface elevation is about 15° (Figure 4b), with the largest discrepancies occurring at COP and BAY stations. These stations are located in shallow bays (mean depth of 2 m) where frictional effects dominate. Thus the model reproduces the variation in amplitude and phase lag throughout the model domain with the largest discrepancies between observed and simulated tides occurring inside the inlet and in the shallow, friction-dominated bays.

4.1.3. Comparison between modeled and observed discharges and velocities. The amplitude and phasing between simulated and observed (ADCP) discharges agree well in the three channels as well as in the entrance channel (Figure 5). During this 3-day period, peak discharges through the inlet are 6000-7000 m^3 s^{-1} (Figure 5a). The majority (~60%) of the flow entering the inlet flows toward Corpus Christi Bay via the CC Ship Channel (Section B), approximately 30% flows toward Aransas Bay via Lydia Ann Channel (Section D), and the remaining 10% flows toward Redfish Bay via Aransas Channel (Section C). The model underpredicts peak flood discharges in the CC Ship Channel by approximately 34% and overpredicts peak ebb discharges in Aransas Channel by 30% (Figure 5b). The RMS difference between observed and simulated discharges are 675, 600, 96,

Table 4. Observed (O.) and Modeled (M.) Current Amplitude (Amp., Major Axis) and Greenwich Phase Lag for Dominant Diurnal and Semidiurnal Tidal Constituents Over the Time Period of April 9 to May 8, 1990

Depth	Type	K_1		O_1		M_2	
		Amp., cm s^{-1}	Lag, deg	Amp., cm s^{-1}	Lag, deg	Amp., cm s^{-1}	Lag, deg
Surface	O.	58.8	8	59.1	13	25.5	285
	M.	71.6	355	83.3	14	26.2	271
Mid	O.	51.3	6	50.8	12	18.7	294
	M.	65.6	354	76.3	14	24.1	272
Bottom	O.	40.1	5	40.0	11	14.9	308
	M.	33.8	354	39.4	13	12.8	271

The bottom-mounted ADCP was located at 27.84°N / 97.04°W (location shown in Figure 2b). Surface, middepth, and bottom currents are located at 1, 7, and 15 m depths, respectively.

and 267 $m^3 s^{-1}$ for sections A, B, C, and D, respectively. Peak flood discharges inside the inlet are in phase with high tides in the Gulf of Mexico (Figure 5a), suggesting that the tide is behaving as a progressive wave.

The model overpredicts the surface and middepth tidal current velocities (major axis) in the ship channel by 20-30% and 40-50% for the K_1 and O_1 constituents, respectively, and 2-30% for the M_2 constituent (Table 4). There is better agreement between model and observed current magnitudes near the bottom. Tidal ellipses inside the inlet are aligned with the channel with minor axes amplitudes of less than 1 cm s^{-1}. The observed current amplitudes (major axis) for the K_1 and O_1 constituents are about 60 cm s^{-1}, while the amplitude of the M_2 currents is about 25 cm s^{-1}. The differences between modeled and observed currents may be associated with representation of the bathymetry in the model and position of the ADCP. Inside the inlet, the tidal energy is rapidly attenuated, and small differences in bathymetry or location can have large effects on calculated or observed velocities.

4.1.4. Description of modeled flow. Peak depth-averaged velocities in the inlet during tropic tides are about 1.5 m s^{-1}. There is an asymmetry in the speed of peak ebb and flood currents in the inlet, with ebb flows that are about 10-30% faster than flood. This relative difference between ebb and flood flows is larger during higher flow conditions. Flood currents are retarded by friction of the shallow water and channel constrictions; however, ebb currents can flow more easily onto the shelf. The stronger ebb currents are balanced by slightly longer flood tides. Peak surface velocities inside the inlet are about 16% higher than bottom velocities during ebb flow and 8-9% higher during flood flow.

The currents on the Gulf of Mexico side of the inlet differ greatly between flood and ebb stages. Flow during flood tide is almost uniformly toward the inlet in the region near the inlet (Figure 6a); flow during ebb tide exits the inlet as a jet (Figure 6b) that is aligned with the channel, extends approximately 5 km from the tip of the jetties, and undergoes minimal lateral expansion. Centerline velocities of the jet decrease almost linearly with distance from the jetties; at 5 km from the jetties the velocities are 10% of their values at the end of the inlet. Two symmetric counterrotating eddies develop on either side of the ebb jet, similar to idealized inlet circulation patterns [*Imasato*, 1983]. These eddies form at the tip of the jetties approximately 3 hours after ebb flow begins. As the jet increases in length, the eddies increase in size and move offshore with the jet. During the subsequent flood tide, the seaward portion of the jet and the eddies persist about 5 km offshore of the inlet. The counterrotating eddies are maintained by the ebb tidal jet and shoreward flow on outermost sides of the eddies during flood tides. Although symmetric eddies are present in depth-averaged velocity fields, the residual circulation patterns (time average of Eulerian velocities over 6 tidal cycles) are asymmetric with a larger southern eddy (length scale of ~10 km) and a northern eddy that is elongated in the cross-shore direction and

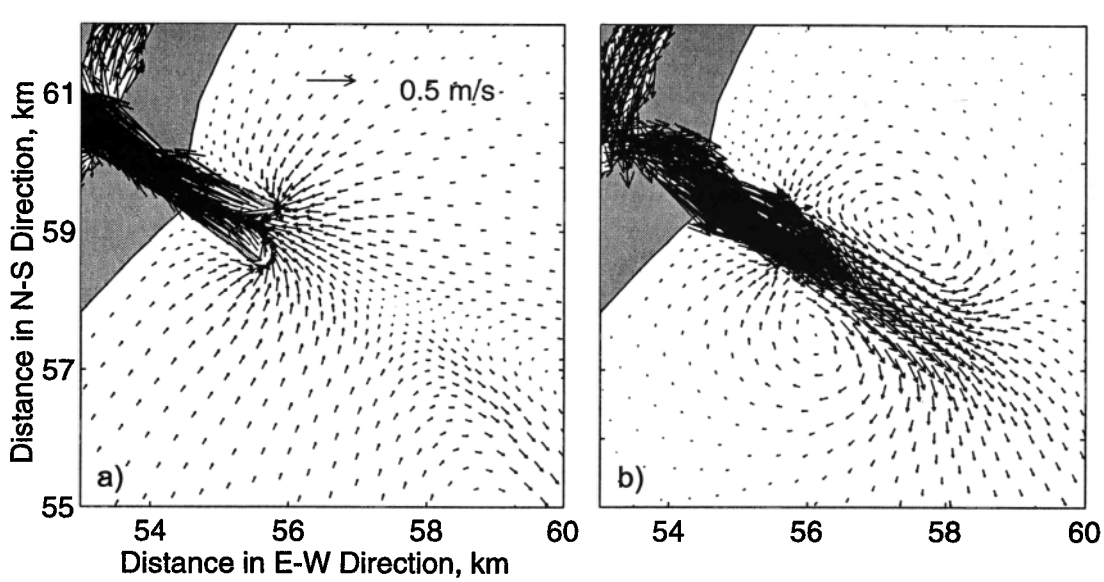

Figure 6. Vertically integrated velocities near the inlet for $K_1 + O_1 + P_1$ forcing during (a) peak flood and (b) peak ebb.

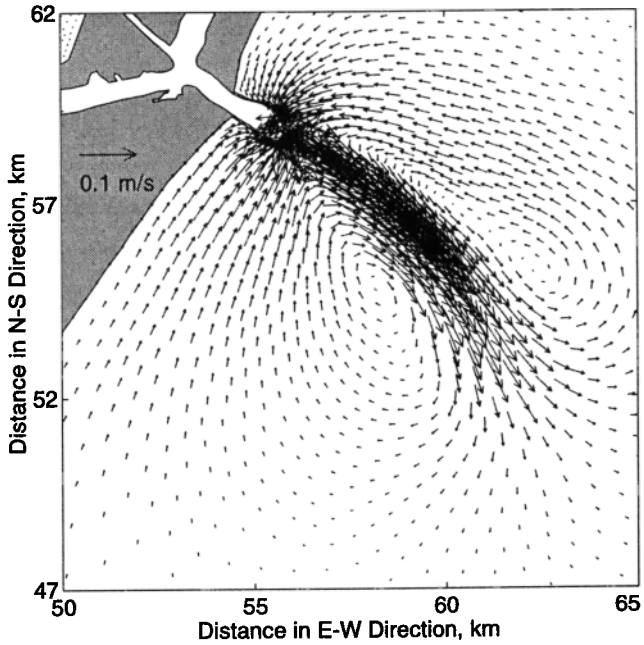

Figure 7. Vertically integrated residual (time average over 5 tidal cycles) circulation pattern outside the inlet.

compressed in the alongshore direction (Figure 7). Maximum residual velocities of about 20 cm s^{-1} are associated with the offshore jet, while the nearshore residual flow toward the inlet has velocities of approximately 5 cm s^{-1}.

4.1.5. Attenuation of tidal constituents within bays and channels. In the Gulf of Mexico adjacent to the study area, the amplitude of each of the dominant diurnal constituents, K_1 and O_1, is approximately 15 cm. As the dominant diurnal tides propagate through the inlet, frictional effects rapidly reduce the amplitudes of each of the constituents to 9-11 cm inside the inlet (Figure 8a). The amplitudes of the dominant diurnal constituents within Corpus Christi Bay are about 6 cm each and are relatively spatially uniform. There is a minor amplification of the K_1 and O_1 constituents within the bay that is evident in both the tidal analysis and the model results (e.g., compare amplitude of ING to that at NAS and AQU). In Redfish Bay, the amplitudes of the K_1 and O_1 constituents are 3.5-5 cm. The amplitude of the diurnal constituents within Aransas Bay are a relatively constant 3 cm, approximately half of that in Corpus Christi Bay. There is a minor amplification of diurnal constituents within Copano Bay (e.g., compare amplitude of COP to that at BAY).

In the Gulf of Mexico, the amplitude of the dominant semidiurnal constituent, M_2, is 8 cm. This semidiurnal constituent is preferentially attenuated (compared with the diurnal components) as it propagates through the channels, resulting in amplitudes of less than 2 cm in Corpus Christi and Redfish Bays and less than 1 cm in Aransas and Copano Bays. There may also be a slight amplification of the M_2 constituent in the bays.

There is a phase lag difference of approximately 60° or 4 hours between Port Aransas and Ingleside for the diurnal constituents and a difference of approximately 100° or 3.5 hours for the semidiurnal constituent (Figure 8b). However, there is essentially no difference (< 4° or 0.3 hour) in phase lag for the dominant diurnal constituents at the four stations located within Corpus Christi Bay (NAS, AQU, THE, and SHA).

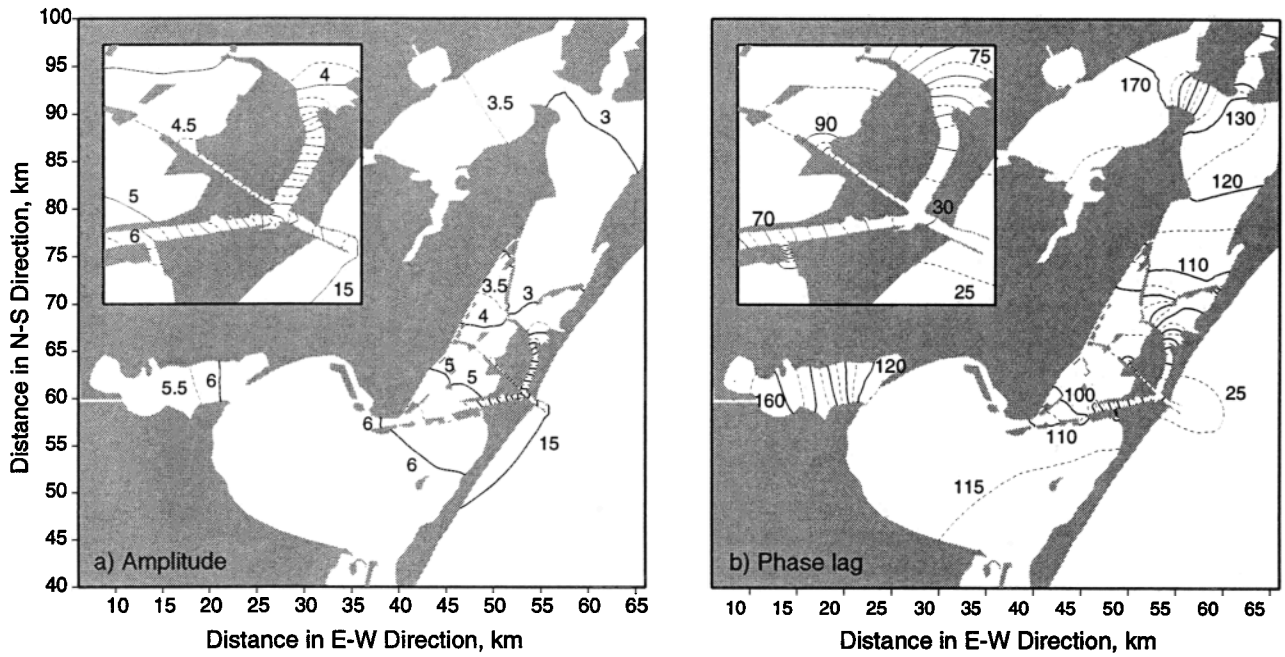

Figure 8. Spatial distribution of (a) amplitude and (b) phase lag of the K_1 constituent. The distribution of the amplitude and the phase lag of the O_1 constituent are similar to those for the K_1 constituent. The majority of the attenuation of the amplitude and retarding of the propagation speed of the tidal motion occurs within the channels leading to the various bays, while inside the bays the amplitudes and phase lags are relatively uniform. The inset shows the changes in amplitude and phase lag in the vicinity of the inlet opening.

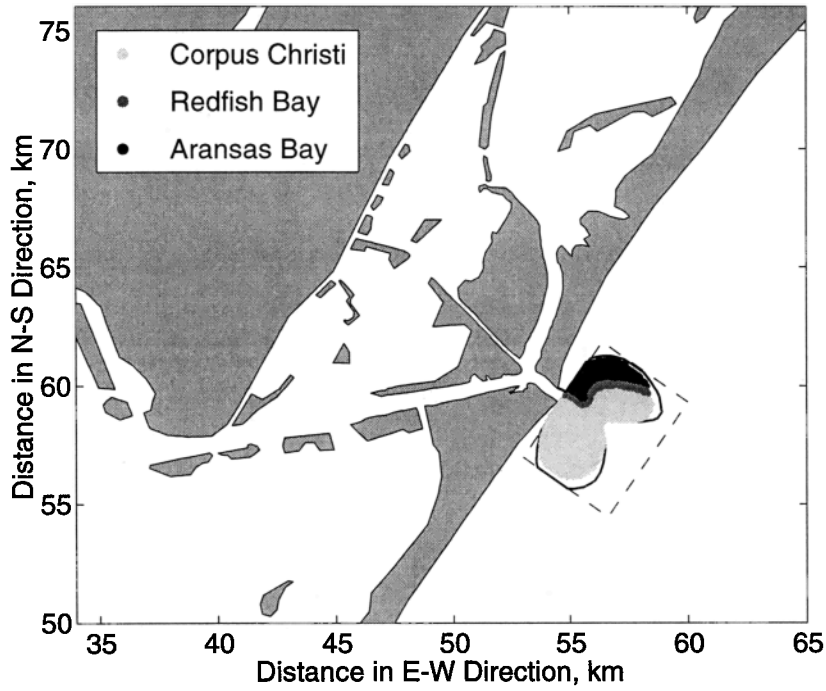

Figure 9. Source region of particles that enter the inlet during initial flood tide under $K_1 + O_1 + P_1$ forcing with particles shaded according to which channel they enter during the first flood tide. The solid line indicates extent of flood water that enters the inlet, and the dashed line indicates the boundary of initial particle release. Particles released south and offshore of the inlet are transported toward Corpus Christi Bay. Particles that are transported toward Aransas Bay are released on the northern side of the inlet.

4.2. Passive Particle Transport

4.2.1. Source of flood waters. Particles that enter the inlet during the first flood tide come from a region that extends approximately 3 km offshore and a similar distance up and down coast of the inlet (Figure 9). The shape of the region is bilobed, not circular, as particles preferentially enter from the sides (~90%) rather than offshore of the inlet. Directly offshore of the inlet, the seaward extent of the source region is closer to shore owing to the persistent offshore flow in the channel (Figure 7). Particles that enter the inlet come mostly from inside the 12-m depth contour. The two source regions up and down the coast of the inlet have slightly different shapes but approximately equal areas. The presence of the jetties displaces the source region offshore compared with an idealized inlet without jetties. During the initial flood tide, 61% (2921 of 4772) of the particles, representing an area of 16.5 km^2, are transported into the inlet landward of Transect A (Figure 2a).

An asymmetry develops in the source region of particles that enter the inlet over multiple tidal cycles (Figure 10a). Over 5 tidal cycles, particles that enter the inlet from south come from a region that is primarily inshore (<5 km from the coast) but extends 10 km south of the inlet. Particles from the south are transported to the inlet by the particularly strong alongshore residual flow (Figure 7). Particles that enter the inlet from the north come from a region that extends about 10 km from the coast but only 4-5 km north. Between the northern and southern source regions, there is a relatively large area to the south and offshore from which particles do not enter the inlet. Particles in this region are entrained in the ebb tidal jet and are transported either offshore or to a region with relatively low velocities in the southern eddy (Figure 7). Despite the asymmetry in their shapes, approximately equal numbers of particles enter the inlet from the regions to the north (45%) and the south (55%) during each tidal cycle. All of the particles that approach the inlet from the south enter the CC Ship Channel. Particles that come from the north enter the CC Ship and Lydia Ann Channels in almost equal proportions.

Simulations were performed to determine the cause of the asymmetry in source location for particles that enter the inlet over 5 tidal cycles. Outside of the inlet there is a shoal south of the inlet (Figure 2c). To examine the local bathymetric effects, the bathymetry of the mesh was modified by removing this shoal. The source location of particles entering the inlet were computed for three cases: (1) existing bathymetry with no Coriolis (i.e., latitude set to 0°), (2) modified bathymetry with Coriolis term included, and (3) modified bathymetry with no Coriolis. Removing rotational effects (case 1) results in a reduction in the asymmetry between the particle source locations north and south of the inlet; however, an asymmetry remains (Figure 10b). The remaining asymmetry is associated with bathymetric affects. There is no asymmetry in particle source location over multiple tidal cycles for case 3 (results not shown).

4.2.2. Maximum inward tidal excursion. For the remainder of this paper, particle transport is discussed for particles released over the smaller region and their transport over 1 tidal cycle (see Figure 9). Maximum inward excursion for passive particles released in the upper part of the water

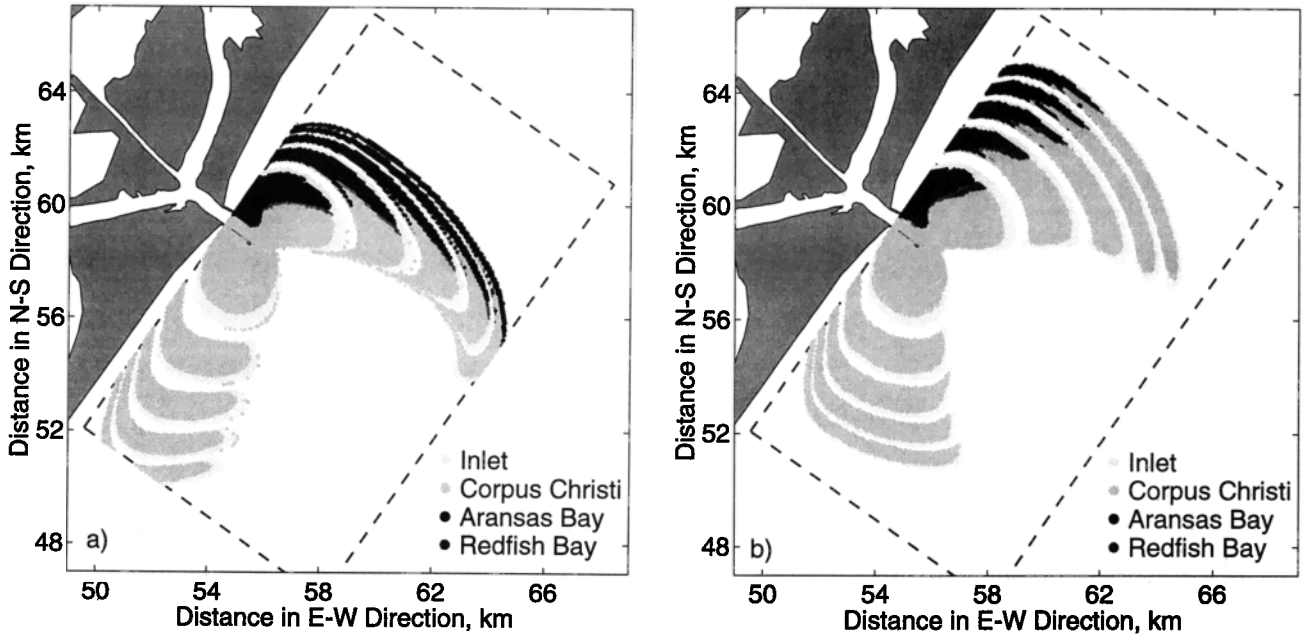

Figure 10. (a) Source region of particles that enter the inlet over 5 tidal cycles with the dashed line indicating the boundary of initial particle release region. Over 5 tidal cycles an asymmetry develops between the upcoast and downcoast sides of the inlet. Particles entering the inlet from the south are obtained from a region that is relatively close to shore (<5 km), while those entering from the north are obtained from a region that extends approximately 10 km offshore. All of the particles entering the inlet from the south are transported toward Corpus Christi Bay, while particles entering the inlet from the north are approximately equally divided between the CC Ship and Lydia Ann Channels. (b) Same as Figure 10a, but computed neglecting Coriolis. The asymmetry between the upcoast and downcoast sides of the inlet is reduced in comparison with that computed including Coriolis (Figure 10a).

column is approximately 15 km beyond the confluence of the three channels (Figure 11). Particles that are transported via the CC Ship Channel are transported as far as Ingleside, while those transported in Lydia Ann Channel are transported to Mud Island.

Approximately 60% of the particles that enter the inlet are transported into the CC Ship Channel (landward of Transect B), 18% are transported into Lydia Ann Channel (landward of Transect D), 3% are transported into the Aransas Channel (landward of Transect C), and the remaining 17% remain in the entrance channel (the region between Transect A and Transects B, C, and D). This division of the transport of the particles between the channels is similar to the division of flow that has been measured by using acoustic Doppler current profilers (Figure 5). Particles transported in the CC Ship Channel originate in the middle and southern portion of the source region, while those transported into Lydia Ann Channel are from a small region north of the inlet (Figure 9). There is little mixing of the particles between the different bays of the study area and little mixing of the particles out of the channels into the bays.

4.2.3. Ebb particle transport. Bay-shelf exchange of particles occurs as a result of the asymmetry between ebbing and flooding currents. As was discussed previously, the source region of flood tides is two almost symmetric regions adjacent to the jetties. The majority of the particles entering on the flood tide are expelled a maximum distance of about 7 km offshore (to the 17-m depth contour) during the subsequent ebb tide in a tidal jet (Figure 12). Most of these particles do not reenter the inlet during the next flood tide because they are seaward of the flood water source region.

Approximately 9% of the particles that enter the inlet remain landward of Transect A after the subsequent ebb tide: 57% of those are in the CC Ship Channel, 32% are in the entrance to the inlet (the region between Transect A and Transects B, C, and D), 10% are in the Aransas Channel, and <1% are in Lydia Ann Channel. Only 5% of the entering particles (141 particles) remain landward of Transect A after 5 tidal cycles: 70% in the CC Ship Channel, 3.5% in Lydia Ann Channel, and 2.8% in the Aransas Channel. Thus a small fraction of those particles that stay inside the inlet are retained in regions with suitable nursery habitat (i.e., Lydia Ann Channel and Redfish Bay). Over multiple tidal cycles, the CC Ship Channel often contains a mixture of particles that originated in different portions of the source regions; however, the only particles in Lydia Ann Channel are those that initially entered this channel. The mixing of the particles from different source regions occurs outside the inlet during the ebb tide.

4.2.4. Effect of varying particle release location. Particle transport and retention within the bays depend upon the location of particle release. Particles released inside the inlet at the beginning of flood tide move further into the bays after a tidal cycle than particles released offshore. In addition, more particles remain landward of the inlet (Transect A) after multiple tidal cycles (Figure 13). About

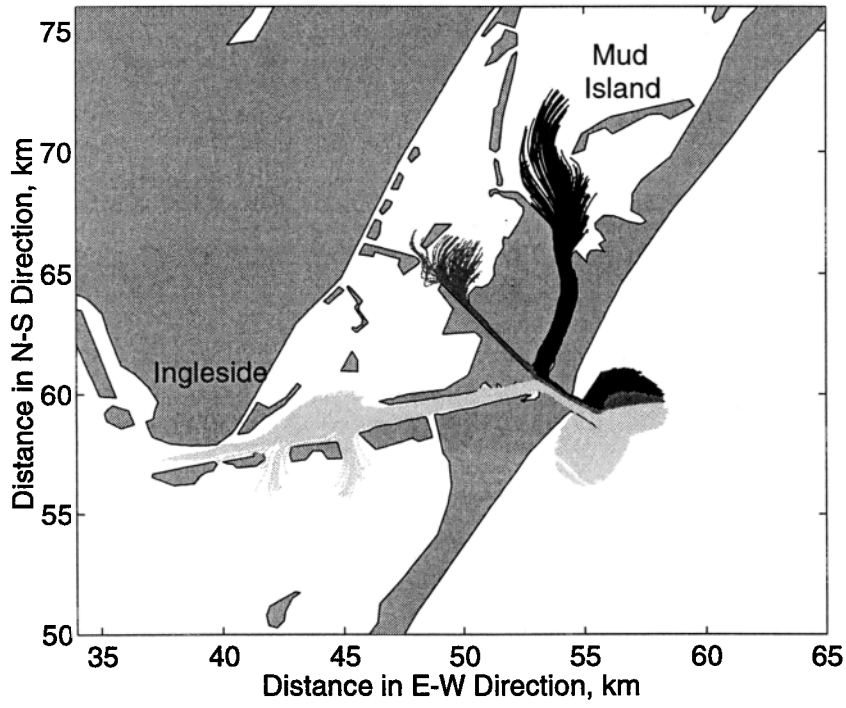

Figure 11. Maximum particle excursions at the end of initial flood tide for particles released at the beginning of flood tide under $K_1 + O_1 + P_1$ forcing. The maximum excursion of particles into the bays extends approximately 10-15 km beyond the confluence of the three channels.

35% of the particles released inside the inlet are expelled offshore after the first tidal cycle compared with 90% for particles released outside the inlet. About 10% of the particles released inside the inlet remain landward of Transect A after 5 tidal cycles, compared with only 5% for particles released outside the inlet.

5. Discussion

Model and analysis results are consistent with the previous published studies of physical processes in the region [e.g., *Smith*, 1974, 1979]. This study benefits from the increased spatial and temporal coverage of water level data available from the TCOON. Previous studies concentrated on the tides within Corpus Christi Bay, while this study also includes Aransas, Redfish, and Copano Bays. The model reproduces variations in amplitude and phase lag of the surface elevation throughout the model domain as well as the magnitude of discharge inside the inlet and each channel. Tidal current velocities (computed from observations of *Williams et al.* [1991] and model results) are about 2-3 times greater than previously published values [*Smith*, 1979]. This discrepancy is due to location of the current measurements used for the analyses. Current observations for the previous study [*Smith*, 1979] were obtained from a current meter deployed 1 m above the bottom along the slope of the ship channel (10-m depth), while the tidal current magnitudes computed in this study were from a bottom-mounted ADCP deployed on the bottom of the ship channel (14-m depth). Several features of the tides that were identified in previous studies are present in the simulations.

Smith [1974] identified a minor amplification of the amplitude and acceleration in the propagation speed of the diurnal components within Corpus Christi Bay. He speculated that these features were associated with coupling between diurnal wind and astronomical tidal forcing or internal tidal generation. Model simulations and analysis confirm the presence of these features of the diurnal components; however, since the model reproduces these features without including either proposed forcing mechanisms, these mechanisms may be eliminated.

The classical view of an idealized, constricted tidal inlet is that inflow has flow lines similar to those for potential flow to an orifice with water coming from a semicircular region near the inlet and outflow forms a momentum-dominated jet [e.g., *Stommel and Farmer*, 1952; *Lee and Rooth*, 1972; *Oertel*, 1988; *Kapolnai et al.*, 1996]. Models of ebb tidal flow based on classical two-dimensional turbulent jets suggest that the jet width expands exponentially with distance offshore for inlets with large aspect ratio (half width of inlet/mean depth) or large frictional momentum losses [*Özsoy and Ünlüata*, 1982]. In our simulations, the minimal expansion of the ebb tidal jet is consistent with the low aspect ratio of the inlet. Our simulations indicate that two symmetric, counterrotating eddies form during ebb flow on either side of the jet, a result that is similar to the circulation patterns for idealized inlets [*Imasato*, 1983; *Chao*, 1990]. These eddies result in an alongshore flow near the jetties and a shoreward flow on their outer flanks that transport water toward the inlet. Particles that enter the inlet after the initial flood tide are moved toward the inlet by these eddies.

Our simulations indicate that the source of flood tide water for Aransas Pass is displaced offshore relative to that for the idealized inlet. Flood water comes from two relatively symmetric regions located on either side of the jetties. Little of the water directly offshore of the inlet enters because of a

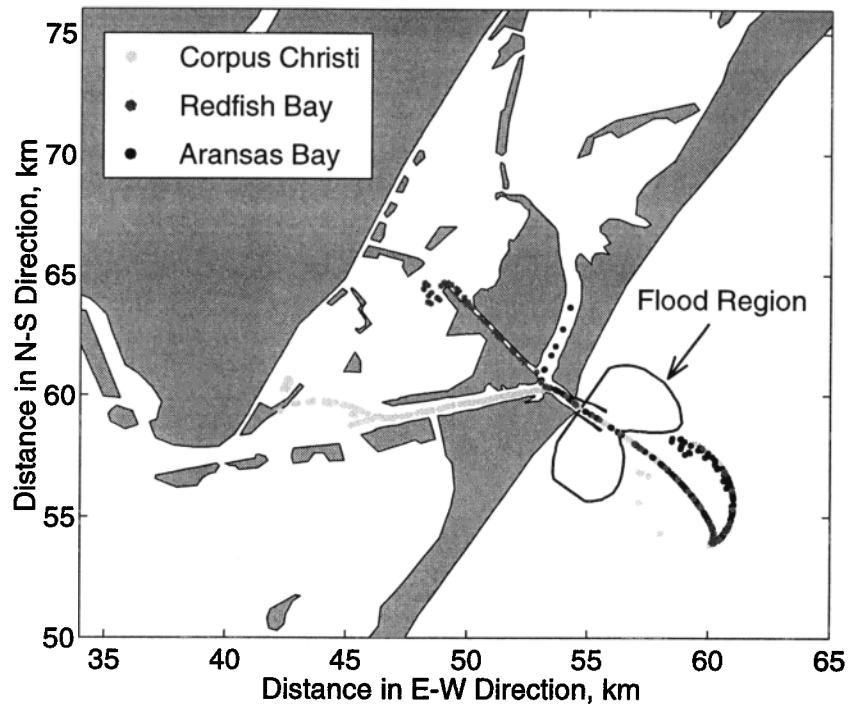

Figure 12. Particle locations at the end of first ebb tide. Most of the particles that enter the inlet are expelled about 7 km offshore in the ebb tidal jet. Most of these particles are expelled beyond the source of flood water and do not reenter the inlet during subsequent flood tides.

persistent offshore flow in the channel associated with the previous ebb tidal jet. *Imasato* [1983] calculated similar persistent offshore flow and eddies for an idealized inlet with low frictional dissipation. The jetties and CC Ship Channel may effectively reduce bottom friction by discharging water further offshore at deeper depths.

Residual circulation patterns indicate that there is an anticyclonic eddy south of the jetties that is larger than the cyclonic eddy to the north, while the northern eddy is elongated in the cross-shore direction. Previous modeling studies of idealized inlets have shown that the anticyclonic eddy is generally stronger than the cyclonic eddy because of the Earth's rotation and offshore sloping bathymetry tends to enhance its strength [*Chao*, 1990]. However, we ran a simulation with the Coriolis term set to zero that shows that the asymmetry in the eddies persists, indicating that this asymmetry is associated with bathymetric features near the inlet combined with rotational effects. There is a shoal south of the inlet (Figure 2c) that contributes to the asymmetry in the residual circulation patterns.

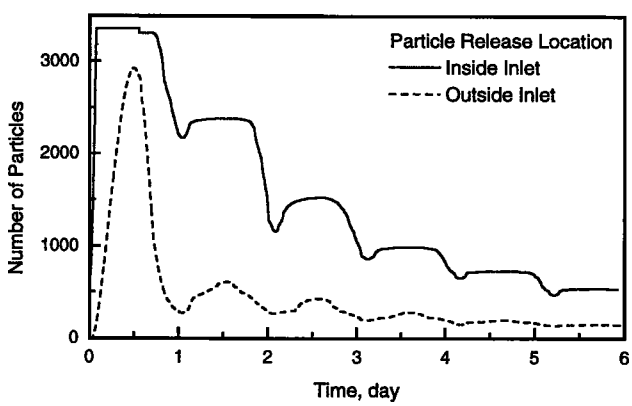

Figure 13. Time series of the number of particles inside the inlet (landward of Transect A) illustrating the effect of release location of the particles on particle retention within the bays. Releasing particles inside the inlet results in more particles being retained within the bay through multiple tidal cycles.

Residual circulation patterns influence particle transport over multiple tidal cycles. Most of the particles in the southern eddy are reentrained in the ebb tidal jet and transported offshore. In the southern eddy, the offshore velocities are stronger than the onshore velocities, while in the northern eddy the onshore velocities are stronger. The northern eddy is more effective at transporting particles onshore toward the inlet because it has larger onshore velocities over a larger area. Trajectories indicate particles in the region southeast of the inlet that do not enter the inlet are either entrained in a strong offshore flow or they move into a region with small residual velocities (<1 cm s^{-1}) rather than being retained in the southern eddy. For comparison, residual circulation patterns for Beaufort Inlet, North Carolina show a single anticyclonic eddy downcoast of the inlet [*Luettich et al.*, 1999]. The differences between residual circulation patterns at Aransas Pass and Beaufort Inlet may be due to bathymetric differences between the two and by the presence of jetties at Aransas Pass, as well as to differences in rotational effects associated with differences in latitude.

Circulation patterns in the vicinity of the inlet are generally consistent with modeling studies of idealized inlets (i.e., no jetties and uniform depth). However, substantial differences from idealized patterns result from bathymetric variations in the vicinity of the inlet and the presence of jetties. Although models of idealized inlets provide important insights into circulation patterns in the vicinity of tidal inlets and particle

transport mechanisms, bathymetric features can substantially modify results and have major implications for larval transport. Models that incorporate realistic bathymetric features specific to the inlet being studied are required for accurate predictions of larval movement.

Although the tidal amplitudes within the study area are relatively small, they account for approximately half of the variance in water level fluctuations outside the inlet, and they provide a regular daily flow through the inlet with peak velocities of the order of 1-1.5 m s^{-1}. Flows with these velocities can transport particles released in the vicinity of the inlet a distance of approximately 10-15 km beyond the confluence of the entrance channels. Tidal excursions estimated on the basis of particle trajectories are consistent with previous estimates based on limited current measurements [*Smith*, 1979].

There is minimal mixing of the particles into Corpus Christi and Aransas Bays because the maximum tidal excursions are comparable to the lengths of the channels. For tidal amplitudes of 6-12 cm (characteristic of equatorial and tropic tides in Corpus Christi Bay) and a surface area for Corpus Christi Bay of 435 km^2 [*Ward*, 1997], the tidal prism of the dominant diurnal tides varies from 25 to 50 x 10^6 m^3. The volume of the CC Ship Channel below natural bay bottom estimated by assuming a trapezoidal shape, channel depth of 13.7 m, channel bottom width of 120 m, channel side slope of 1:2, mean bay depth of 3.6 m, and a channel length of 35 km is about 50 x 10^6 m^3. Thus the volume of the CC Ship Channel is 1-2 times volume of the tidal prism; water that enters the inlet stays within the CC Ship Channel and has limited excursions into Corpus Christi Bay. The islands to the south of the CC Ship Channel may further reduce the mixing of particles within the bay by minimizing the interactions between bay and channel waters. Thus particles that are transported into the CC Ship Channel tend to remain in this channel.

Abrupt changes in bathymetry and coastline geometry often generate complex spatial patterns in tidal currents that increase tidal dispersion within bays and facilitate bay-shelf exchange [*Geyer and Signell*, 1992; *Zimmerman*, 1986]. Tidal dispersion is enhanced in regions where the spacing between major topographic features is less than the tidal excursion distance and in regions where flow separation occurs, such as near tidal inlets and headlands [*Geyer and Signell*, 1992; *Signell and Geyer*, 1990]. However, in the vicinity of Aransas Pass the length scale of the tidal excursion is similar to the length scale of the channels, which restricts the dispersion of particles within the bays. Inside the bays there is minimal tidal dispersion of particles because the tidal excursion is small owing to limited tidal forcing. The majority of the particles that are retained landward of the inlet through multiple tidal cycles remain within the CC Ship Channel and are not dispersed into Corpus Christi and Aransas bays.

Larvae depend upon currents to transport them through the inlet and to a suitable habitat. Owing to the time required for larval development, the timing of the larval transport to an estuarine habitat is an important factor in recruitment. If larvae are transported to a suitable settlement habitat but are insufficiently developed ("precompetent phase"), they will not be able to respond to the environment and settle. A significant source of larval mortality may be associated with larvae being transported away from a suitable settlement habitat during this precompetent phase and their inability to reach a suitable habitat when they are competent [*Jackson and Strathmann*, 1981].

Red drum spawn from late August to early October in the northwestern Gulf of Mexico [*Holt et al.*, 1985]. Red drum produce buoyant eggs that are 1-mm in diameter and hatch about 24 hours after spawning [*Holt et al.*, 1985]. The larvae have a precompetent phase of about 20 days, at the end of which they have grown to an average standard length of 8 mm [*Holt et al.*, 1983; *Rooker et al.*, 1999]. Sea grass beds serve as the nursery grounds for red drum [*Holt et al.*, 1983; *Rooker and Holt*, 1997]. In the Aransas Pass region, sea grass beds are primarily located in Redfish Bay, south of Mud Island on the back side of the barrier island, and along the edges of Lydia Ann Channel [*Pulich et al.*, 1997]. The need to be near an appropriate habitat if they are to continue to grow upon becoming competent makes the current patterns an important part of their life histories.

Particle trajectories depend upon the location of particle release. Our simulations show that, under tidal forcing conditions, pathways to different bays have distinct source regions. Particles entering the inlet during the first flood tide are equally divided between the source regions to the northeast and southwest of the jetties; however, particles transported to regions with a sea grass habitat come preferentially from the region to the northeast of the jetties. The greater flow of the CC Ship Channel moves most particles toward Corpus Christi Bay, a region with little suitable estuarine habitat for settlement. The spatially distinct source regions for transport to the different bays illustrates the importance of knowing the adult spawning location and spatial distribution of larvae in the vicinity of the inlet. Based on the presence of eggs and drumming noises associated with courtship, it is known that a portion of the red drum population spawn in the vicinity of the tidal inlet [*Holt et al.*, 1989]. The presence of eggs (2-4 hours old) in flood waters and their absence in ebb waters indicate that a portion of the red drum population spawn in the Gulf near Aransas Pass [*Holt et al.*, 1989]; however, the exact location of spawning and the degree of alongshore transport of eggs and larvae are unknown. Our simulations suggest that the location of spawning and cross-channel variability in larval abundance may have large impacts on larval transport to suitable estuarine habitat. The spatially distinct source regions of flood waters for the bays should be taken into consideration in the design of larval sampling studies. This is particularly important for bay-inlet systems with branched channels leading to multiple bays, especially if there are differences in distribution or quality of nursery habitat between the bays.

Barotropic tidal forcing is effective at transporting larvae a distance of 10-15 km into the bays; however, when acting alone, tidal forcing is not effective at maintaining passive larvae within the bays and regions with suitable nursery habitat. The majority of particles entering the bays during flood tide are exported offshore during the subsequent ebb tide by the tidal jet, suggesting that if they do stay, other physical or biological mechanisms are required to maintain them within the bays, such as mixing (e.g., local wind forcing or subgrid scale motions) or behavior. Once ejected offshore, larvae may be transported away from the inlet by alongshore currents, including wave-generated longshore currents and larger-scale, along-shelf flow. The Texas shelf is dominated by downcoast flow throughout the year except during the

summer months of July and August [*Cochrane and Kelly*, 1986]. Assuming a precompetent period of 2 weeks and a typical alongshore current of 10 cm s^{-1} [*DiMarco et al.*, 1997], larvae could be advected about 120 km, which is comparable to the length scale between inlets in this portion of the Gulf of Mexico. The dominance of the ebb tidal jet on circulation patterns near the inlet suggests that there may be substantial transport of larvae down the coast.

There is an asymmetry between the north and south sides of the jetty in particles that enter the inlet over multiple tidal cycles. This asymmetry is not present in a previous model study of an idealized inlet [*Kapolnai et al.*, 1996] and is associated with rotational and bathymetric effects. The asymmetry in the source region of particles that enter the inlet suggests that larvae that approach the inlet from the north are more effectively transported to a suitable habitat. In addition, a northern approach is more effective if the larvae need to be transported across the shelf toward the inlet owing to the stronger onshore residual flows over a larger area.

This paper represents the first part of a study to identify the role of physical and biological processes influencing larval transport through Aransas Pass. We are systematically introducing complexity by incorporating additional forcing (such as wind stress, baroclinic, and low-frequency water level fluctuations associated with larger-scale shelf circulation patterns) and larval behavior (e.g., vertical migration and settlement).

Acknowledgments. This study was funded by Institutional Grant NA86RG0058 to Texas Sea Grant College Program by NOAA, U.S. Dept. of Commerce. We would like to thank A. Amos for providing tidal constituents for UTMSI Pier, R. Bourgerie for providing NOS data, N. Scheffner for providing ADCIRC results, R. Solis for providing ADCP data, and the reviewers whose comments improved this paper. G. J. Holt, S. A. Holt, R. O. Reid, S. F. DiMarco, J. L. Hench, and R. A. Luettich have provided helpful discussions.

References

Blanton, B. O., DROG3D: User's manual for 3-dimensional drogue tracking on a finite element grid with linear finite elements, 13 pp., Program in Mar. Sci., Univ. of N. C., Chapel Hill, 1995.

Chao, S.-Y., Tidal modulation of estuarine plumes, *J. Phys. Oceanogr., 20*, 1115-1123, 1990.

Cochrane, J. D., and F. J. Kelly, Low-frequency circulation on the Texas-Louisiana continental shelf, *J. Geophys. Res., 91*(C9), 10,645-10,659, 1986.

Colby, D. R., Null hypotheses, models, and statistical designs in the study of larval transport, *Am. Fish. Soc. Symp., 3*, 149-162, 1988.

Cowen, R. K., Large scale pattern of recruitment by the laprid, *Semicossyphus pulcher*: Causes and implications, *J. Mar. Res., 43*, 719-742, 1985.

DiMarco, S. F., and R. O. Reid, Characterization of the principal tidal current constituents on the Texas-Louisiana shelf, *J. Geophys. Res., 103*(C2), 3093-3109, 1998.

DiMarco, S. F., A. E. Jochens, and M. K. Howard, *LATEX Shelf Data Report, Current Meter Moorings, April 1992-December 1994, vol. 1, Introduction, Collection, and Processing, Tech. Rep. 97-01-T*, Dep. of Oceanogr., Tex. A&M Univ., College Station, 1997.

Foreman, M. G. G., Manual for tidal heights analysis and prediction, *Pac. Mar. Sci. Rep. 77-10*, 97 pp., Inst. of Ocean Sci., Patricia Bay, Sidney, B. C., Canada, 1977.

Foreman, M. G. G., Manual for tidal currents analysis and prediction, *Pac. Mar. Sci. Rep. 78-6*, 97 pp., Inst. of Ocean Sci., Patricia Bay, Sidney, B. C., Canada, 1978.

Galperin, B., L. H. Kantha, S. Hassid, and A. Rosati, A quasi-equilibrium turbulent energy model for geophysical flows, *J. Atmos. Sci., 45*, 55-62, 1988.

Geyer, W. R., and R. P. Signell, A reassessment of the role of tidal dispersion in estuaries and bays, *Estuaries, 15*, 97-108, 1992.

Hamer, P. A., and G. P. Jenkins, Larval supply and short-term recruitment of a temperate zone demersal fish, the King George whiting, *Sillaginodes punctata* Cuvier and Valenciennes, to an embayment in south-eastern Australia, *J. Exp. Mar. Biol. Ecol., 208*, 197-214, 1997.

Holt, G. J., S. A. Holt, and C. R. Arnold, Diel periodicity of spawning of sciaenids, *Mar. Ecol. Prog. Ser., 27*, 1-7, 1985.

Holt, S. A., C. L. Kitting, and C. R. Arnold, Distribution of young red drums among different sea-grass meadows, *Trans. Am. Fish. Soc., 112*, 267-271, 1983.

Holt, S. A., G. J. Holt, and C. R. Arnold, Tidal stream transport of larval fishes into non-stratified estuaries, *Rapp. P.-V. Reun. Cons. Int. Explor. Mer, 191*, 100-104, 1989.

Hoss, D. E., and G. W. Thayer, The importance of habitat to the early life history of estuarine dependent fishes, *Am. Fish. Soc. Symp., 14*, 147-158, 1993.

Imasato, N., What is tide-induced residual current?, *J. Phys. Oceanogr., 13*, 1307-1317, 1983.

Jackson, G. A., and R. R. Strathmann, Larval mortality from offshore mixing as a link between precompetent and competent periods of development, *Am. Nat., 118*(1), 16-26, 1981.

Jenkins, G. P, and K. P. Black, Temporal variability in settlement of coastal fish (*Sillaginodes punctata*) determined by low-frequency hydrodynamics, *Limnol. Oceanogr., 39*, 1744-1754, 1994.

Jenkins, G. P, K. P. Black, M. J. Wheatley, and D. N. Hatton, Temporal and spatial variability in recruitment of a temperate, seagrass-associated fish is largely determined by physical processes in the pre- and post-settlement phases, *Mar. Ecol. Prog. Ser., 148*, 23-35, 1997.

Kapolnai, A., F. E. Werner, and J. O. Blanton, Circulation, mixing and exchange processes in the vicinity of tidal inlets: A numerical study, *J. Geophys. Res., 101*(C6), 14,253-14,268, 1996.

Lee, T. N., and C. Rooth, Exchange processes in shallow estuaries, *Sea Grant Spec. Bull. 4*, 33 pp., Univ. of Miami, Miami, Fla., 1972.

Luettich, R. A., J. L. Hench, C. D. Williams, B. O. Blanton, and F. E. Werner, Tidal circulation and larval transport through a barrier island inlet, in *Proceedings of the 5th International Estuarine and Coastal Modeling Conference*, edited by M. L. Spaulding and A. F. Blumberg, pp. 849-863, Am. Soc. of Civ. Eng., Reston, Va., 1998.

Luettich, R. A., J. L. Hench, C. W. Fulcher, F. E. Werner, B. O. Blanton, and J. H. Churchill, Barotropic tidal and wind driven larvae transport in the vicinity of a barrier island inlet, *Fish. Oceanogr., 8* suppl. 2, 190-209, 1999.

Lynch, D. R., and F. E. Werner, Three-dimensional hydrodynamics on finite elements, II, Non-linear time-stepping model, *Int. J. Numer. Methods Fluids, 12*, 507-533, 1991.

Lynch, D. R., J. T. C. Ip, C. E. Namie, and F. E. Werner, Comprehensive coastal circulation model with application to the Gulf of Maine, *Cont. Shelf Res., 16*, 875-906, 1996.

Marmer, H., Tides and sea level in the Gulf of Mexico, *Fish. Bull. Fish Wildlife Serv., 55*, 101-118, 1954.

McHugh, J. L., Estuarine fisheries: Are they doomed?, in *Estuarine Processes*, vol. I, *Uses, Stresses, and Adaptation to the Estuary*, edited by M. Wiley, pp. 15-27, San Diego, Calif., 1976.

Mellor, G. L., and T. Yamada, Development of a turbulence closure model for geophysical fluid problems, *Rev. Geophys., 20*, 851-875, 1982.

Michaud, P. R., C. I. Thurlow, and G. A. Jeffress, Collection and dissemination of marine information from the Texas coastal ocean observation network, in *Proceedings of the U.S. Hydrographic Conference*, Spec. Publ. 32, pp. 168-173, Hydrogr. Soc., Norfolk, Virg.,1994.

Norcross, B. L, and R. F. Shaw, Oceanic and estuarine transport of fish eggs and larvae: A review, *Trans. Am. Fish. Soc., 113*, 153-165, 1984.

Oertel, G. F., Processes of sediment exchange between tidal inlets, ebb deltas and barrier islands, in *Hydrodynamics and Sediment Dynamics of Tidal Inlets*, Coastal Estuarine Stud., vol. 29, edited by W. L. Aubrey and L. Weishar, pp. 297-318, Springer-Verlag, New York, 1988.

Özsoy, E., and Ü. Ünlüata, Ebb-tidal flow characteristics near inlets, *Estuarine Coastal Shelf Sci., 14*, 251-263, 1982.

Powell, G. L., J. Matsumoto, W. L. Longley, and D. A. Brock, Effects of structures and practices on the circulation and salinity patterns of the Corpus Christi Bay National Estuary Program area, Texas, *Tech. Rep. CCBNEP-19*, 169 pp., Tex. Nat. Resour. Conserv. Comm., Austin, 1997.

Pulich, W., Jr., C. Blair, and W. A. White, Current status and historical trends in seagrasses in the Corpus Christi Bay National Estuary Program Study Area, *Tech. Rep. CCBNEP-20*, Tex. Nat. Resour. Conserv. Comm., Austin, 1997.

Reid, R. O., Tides and storm surges, in *Handbook of Coastal and Ocean Engineering*, vol. 1, edited by J. B. Herbick, pp. 533-590, Gulf, Houston, Tex., 1990.

Reid, R. O., and R. E. Whitaker, *Numerical Model for Astronomical Tides in the Gulf of Mexico*, vol. 1, *Theory and Application*, 115 pp., Tex. A&M Univ., College Station, 1981.

Rooker, J. R., and S. A. Holt, Utilization of subtropical seagrass meadows by newly settled red drum *Sciaenops ocellatus*: Patterns of distribution and growth, *Mar. Ecol. Prog. Ser., 158*, 139-149, 1997.

Rooker, J. R., S. A. Holt, G. J. Holt, and L. A. Fuiman, Spatial and temporal variability in growth, mortality, and recruitment potential of postsettlement red drum, *Sciaenops ocellatus*, in a subtropical estuary, *Fish. Bull., 97*, 581-590, 1999.

Roughgarden, J., S. Gaines, and H. Possingham, Recruitment dynamics in complex life cycles, *Science, 241*, 1460-1466, 1988.

Signell, R. P., and W. R. Geyer, Numerical simulation of tidal dispersion around a coastal headland, in *Residuals Currents and Long-Term Transport in Estuaries and Bays*, Coastal Estuarine Stud., vol. 38, edited by R. T. Cheng, pp. 210-222, Springer-Verlag, New York, 1990.

Smagorinsky, J., General circulation experiments with the primitive equations, I, The basic experiment, *Mon. Weather Rev., 91*, 99-164, 1963.

Smith, N. P., Intracoastal tides of Corpus Christi Bay, *Contrib. Mar. Sci., 18*, 205-219, 1974.

Smith, N. P., Intracoastal tides of Upper Laguna Madre, Texas, *Tex. J. Sci., 30*(1), 85-95, 1978.

Smith, N. P., Tidal dynamics and low-frequency exchanges in Aransas Pass, Texas, *Estuaries, 2*, 218-227, 1979.

Smith, N. P., and A. W. Stoner, Computer simulation of larval transport through tidal channels: Role of vertical migration, *Estuarine Coastal Shelf Sci., 37*, 43-58, 1993.

Stommel, H., and H. G. Farmer, On the nature of estuarine circulation, part I, chap. 3 and 4, *Ref. 52-88*, Woods Hole Oceanogr. Inst., Woods Hole, Mass., 1952.

Ward, G. H., Processes and trends of circulation within the Corpus Christi Bay National Estuary Program study area, *Tech. Rep. CCBNEP-21*, 286 pp., Tex. Nat. Resour. Conserv. Comm., Austin, 1997.

Werner, F. E., R. I. Perry, R. G. Lough, and C. E. Naime, Trophodynamics and advective influences on Georges Bank larval cod and haddock, *Deep Sea Res.*, Part. *II, 43*, 1793-1822, 1996.

Werner, F. E., J. A. Quinlan, B. O. Blanton, and R. A. Luettich, The role of hydrodynamics in explaining variability in fish populations, *J. Sea Res., 37*, 195-212, 1997.

Werner, F. E., B. O. Blanton, J. A. Quinlan, and R. A. Luettich, Physical oceanography of the North Carolina continental shelf during the fall and winter seasons: Implications to the transport of larval menhaden, *Fish. Oceanogr., 8* suppl. 2, 7-21, 1999.

Westerink, J. J., R. A. Luettich, and N. W. Scheffner, ADCIRC: An advanced three dimensional circulation model for shelves, coasts and estuaries report 3: Development of a tidal constituent data base for the western North Atlantic and Gulf of Mexico, *Tech. Rep. DRP-92-6*, Coastal Eng. Res. Cent., U.S. Army Eng. Waterw. Exp. Stn., Vicksburg, Miss., 1993.

Wheless, G. H., and A. Valle-Levinson, A modeling study of tidally driven estuarine exchange through a narrow inlet onto a sloping shelf, *J. Geophys. Res., 101*(C11), 25,675-25,687, 1996.

Williams, R. G., T. D. Bethem, G. W. French, and H. R. Frey, Corpus Christi Bay current prediction quality assurance miniproject, *NOAA Tech. Memo. NOS OMA 60*, Natl. Oceanic and Atmos. Admin., Rockville, Md., 1991.

Xie, L., and D. B. Eggleston, Computer simulations of wind-induced estuarine circulation patterns and estuary-shelf exchange processes: The potential role of wind forcing on larval transport, *Estuarine Coastal Shelf Sci., 49*, 221-234, 1999.

Zetler, B. D., and D. V. Hansen, Tides in the Gulf of Mexico-A review and proposed program, *Bull. Mar. Sci., 20*, 57-69, 1970.

Zimmerman, J. T .F., The tidal whirlpool: A review of horizontal dispersion by tidal and residual currents, *Neth. J. Sea Res., 20*(2/3), 133-154, 1986.

D. A. Brooks, C.A. Brown, and G. A. Jackson, Department of Oceanography, Texas A&M University, College Station, TX 77843-3146. (dbrooks@ocean.tamu.edu; cbrown@ocean.tamu.edu; gjackson@tamu.edu)

(Received January 3, 2000; revised July 17, 2000; accepted July 27, 2000.)